Warjito; Prakoso, Aji Putro; Adanta, Dendy; Budiarso; Irwansyah, Ridho

Article

Approach for a breastshot waterwheel numerical simulation methodology using six degrees of freedom

Energy Reports

Provided in Cooperation with:
Elsevier

Suggested Citation: Warjito; Prakoso, Aji Putro; Adanta, Dendy; Budiarso; Irwansyah, Ridho (2020) : Approach for a breastshot waterwheel numerical simulation methodology using six degrees of freedom, Energy Reports, ISSN 2352-4847, Elsevier, Amsterdam, Vol. 6, Iss. 2, pp. 611-616,
https://doi.org/10.1016/j.egyr.2019.11.127

This Version is available at:
https://hdl.handle.net/10419/243940

Available online at www.sciencedirect.com
ScienceDirect
Energy Reports 6 (2020) 611–616
www.elsevier.com/locate/egyr

The 6th International Conference on Power and Energy Systems Engineering (CPESE 2019), 20–23 September 2019, Okinawa, Japan

Approach for a breastshot waterwheel numerical simulation methodology using six degrees of freedom

Warjito, Aji Putro Prakoso, Dendy Adanta, Budiarso, Ridho Irwansyah*

Mechanical Engineering Department, Faculty of Engineering Universitas Indonesia, Kampus Baru UI, Depok 16424, Indonesia

Received 14 October 2019; accepted 23 November 2019

Abstract

Breastshot waterwheels are suitable for low head conditions in power plants because they have more stable efficiency than other types of turbines do. In some cases, computational fluid dynamics (CFD) methods have been utilised for the performance prediction, geometry optimisation or determination of physical phenomena of a breastshot waterwheel because such approaches offer efficiency in terms of energy, time and cost. However, the dynamic approach of the CFD method is different from that in real conditions. For improving the accuracy of CFD simulation results, a feature of 6-degrees of freedom (6-DoF) can be an alternative. This study presented the CFD method using the 6-DoF feature in a breastshot waterwheel. Based on the grid convergence index (GCI) and timestep convergence index (TCI) concepts, 123 000 elements of mesh and a timestep size of 0.002 s were used in this simulation because these parameters fulfilled the GCI and TCI maximum thresholds. The preload values were varied in the simulation, with levels of 75 N·m, 150 N·m, 225 N·m and 300 N·m. Based on the results, the rotation and torque produced by the wheel resulted in a transient period until they naturally became steady. (The rotation and torque were stable). This is the real-world phenomenon of the energy conversion process in a breastshot waterwheel, which cannot be calculated by other features in the CFD method. Thus, the 6-DoF feature can be a suitable option for breastshot waterwheel turbine simulations for performance prediction, geometry optimisation or studying physical phenomena.

Peer-review under responsibility of the scientific committee of the 6th International Conference on Power and Energy Systems Engineering (CPESE 2019).

Keywords: Breastshot; Waterwheel; Computational fluid dynamics method; Six-degrees of freedom

1. Introduction

The global emission-reduction commitment due to environmental concerns has indirectly led to the accelerated development of low-emission power plants, such as hydropower plants [1]. Consequently, many new hydropower plants have been developed over the past years [2]. The development of low-head (<5 m) hydraulic machines is an interesting field of research to develop because of its high potential and easy accessibility [3]. The waterwheels, especially breastshot waterwheels, are one of several hydraulic turbines that normally work in low head conditions

* Corresponding author.
E-mail address: ridho@eng.ui.ac.id (R. Irwansyah).

https://doi.org/10.1016/j.egyr.2019.11.127

Peer-review under responsibility of the scientific committee of the 6th International Conference on Power and Energy Systems Engineering (CPESE 2019).

Table 1. The breastshot waterwheel geometry parameters.

Parameter	Value	Unit	Parameter	Value	Unit
Outer radius (R_O)	1.04	m	Inner radius (R_I)	0.67	m
Bucket depth (d)	0.37	m	Wheel width (B)	0.25	m
Filling ratio (ε)	0.5		Water entry angle (α)	26	degrees
Relative entry angle (γ)	50.9	degrees	Stick angle (β)	120	degrees
Lower section radius (R_A)	0.37	m	Straight stick length (l)	0.26	m

[4,5]. Unfortunately, there is still a lack of breastshot waterwheel utilisation in hydropower plants because this turbine's efficiency is slightly lower than the efficiencies of other types of turbines.

Several studies have been conducted for improving the breastshot turbine performance. Gotoh et al. [6] investigated the difference between the breastshot waterwheel and undershot waterwheel according to their working procedures. Muller and Wolter [7] increased the efficiency of the breastshot system by improving (changing) the ratio of the in- and outflow geometries, which increased the efficiency by 10%. Furthermore, the results of the assessment showed that the breastshot waterwheel is harmless to aquatic biota [7]. Quaranta and Revelli [8] analytically described the factors (losses) that can affect the performance of a breastshot waterwheel. Moreover, Quaranta and Revelli [9,10] conducted a series of experiments to obtain configuration inflows with an efficiency target of more than 80%. Quaranta and Revelli [9,10] also conducted a study of the optimum blade number and configuration in the turbines. However, this study needs to be improved for obtaining an empirical equation to determine the blade number. These researchers also optimised the blade shapes using the CFD method [11]. Warjito et al. [12] and Budiarso et al. [13] conducted a study of the effect of blade number and water energy kinetics (EK) on performance carried out using analysis of variance (ANOVA), and they concluded that these parameters influence turbine performance.

Currently, the use of CFD to predict the performance of breastshot waterwheels is becoming more popular. Furthermore, almost all the literature reviewed above uses the CFD method. However, the dynamic approach of CFD is still different from real or experimental conditions because the rotation of the wheel or runner is a boundary condition in the CFD method, whereas in the real condition, this is a measured result. For improving the accuracy of the results of the CFD method, 6 degrees of freedom (6-DoF) can be used as an alternative method because the rotation of the turbine is a result of numerical calculation. However, in previous research, the 6-DoF feature has not been comprehensively used in the context of breastshot waterwheels [13]. Thus, this study presents the CFD method using the 6-DoF feature in a breastshot waterwheel. It is expected that this method can serve as a reference for numerical breastshot waterwheel simulations so that phenomena of flow physics can be precisely visualised and studied more comprehensively.

2. Methodology

2.1. Geometry

The geometry of the breastshot waterwheel in this study was adopted from the real conditions at a pico-hydro turbine testing facility, Mechanical Engineering Department, Faculty of Engineering, Universitas Indonesia. This waterwheel has 1 m of available head and an available water discharge of 0.05 m^3/s. The geometry of the waterwheel is described inside Table 1, while the location of the mentioned geometry parameters is depicted in Fig. 1.

2.2. Simulation setup

The CFD simulation was performed in ANSYS™ Fluent® 18.2 software. The transient CFD simulation ran in a 5-s simulation time divided into 10 000 timesteps. The gravitational acceleration was turned on in the y-axis direction, where $g_y = -9.81\ m/s^2$. For multiphase modelling, an implicit volume of fluid model was used with an implicit body force. Water was defined as the main phase, with constant surface tension modelling of 0.0728 N/m. The standard k-ε turbulence modelling was used because this provides sufficient precision for predicting the flow pattern in an open channel, such as a breastshot waterwheel [14]. The inlet and outlet were defined as pressure outlets, where the total pressure was 490.5 Pa for the inlet and 0 Pa for the outlet. The default ANSYS turbulence

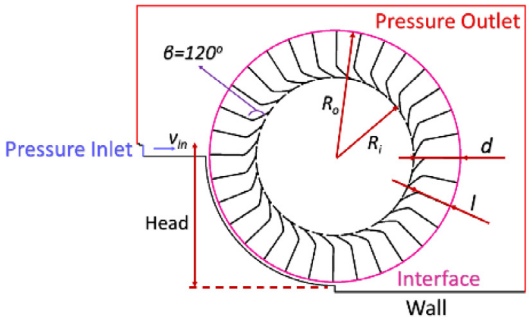

Fig. 1. Dimensions and boundary locations.

specification for inlet and outlet was used in this simulation. The backflow setting of the air phase in the outlet should be turned to 1 to ensure there is no water coming in except from the inlet. The standard interface setting has been used to connect the rotating and static regions in this simulation case. The default wall setting has been used for all walls in this case, including the waterwheel's bucket.

To use the 6-DoF feature in ANSYS, the dynamic mesh option is enabled [15]. For the settings, the 6-DoF option enabled in this simulation was the rotational 1-DoF scheme with 125 kg m^2 of moment inertia. The preload option was turned on as Prony-Brakes loads in the experimental condition. Like Prony-Brakes in experimental testing, the preload in the simulation was varied to values of 75 N m, 150 N m, 225 N m and 300 N m. The motion history should be saved in the correct space in the dynamic mesh option to obtain the angular velocity of the waterwheel at a certain time. The 6-DoF function is then assigned to the rotating domain, including the waterwheel, interface and interior. The passive option was turned off only for the waterwheel boundary.

The SIMPLE scheme for pressure–velocity coupling was used as the simplest and most stable scheme for dynamic simulation. The standard least square cell-based method was used for gradient discretisation as the default method in Fluent. The body force-weighted scheme was used for pressure discretisation which another schemes would result error in calculation. Other variables discretisation including the transient formulation scheme were set as first-order discretisation. The first-order discretisation method is a promising, stable calculation process; however, a finer mesh is needed to obtain a good result. The initial value in this simulation was based on the inlet, but with a value of 1 in the air volume fraction.

2.3. Simulation independency tests

The size of mesh and timestep in dynamic transient CFD simulation is affecting the results of CFD simulations [2]. Before the simulation data is processed, the independency test was performed in order to obtain the optimum size of mesh and timestep. The size of the mesh and timestep in dynamic transient CFD simulation affects the simulation results [2]. Before the simulation data were processed, the independency test was performed to determine the optimum mesh size and timestep.

The independency tests were divided into two stages — mesh independency and timestep independency. The mesh independency tests involved testing the same case with different numbers of mesh elements. The numbers of mesh elements tested were about 30 000 of mesh elements normalised using NGS (Normalised Grid Spacing) to 4, 123 000 to 2 and 493 000 to 1. In the mesh independency tests, the waterwheel was kept static to accelerate the testing process. The Richardson extrapolation method was used for obtaining the appropriate number of mesh elements. In this method, the ratio of mesh refinement is cultivated as constantly as possible. The result of Richardson extrapolation is the grid convergence index (GCI). The GCI is the error index of the tested value from the extrapolated value by the extrapolation process. Normally, the higher the number of mesh elements, the smaller the GCI error will be. The acceptable GCI value for good CFD simulation based on prior studies is below 2%. The mesh quality can also affect the simulation process. This study used a high-quality mesh form with a skewness of 0.4.

The timestep independency stage involved comparing the simulation results with different timestep sizes from 0.002 s normalised (NTS) to 1, 0.004 s to 2 and 0.008 s to 4. The timestep independency tests adopted the

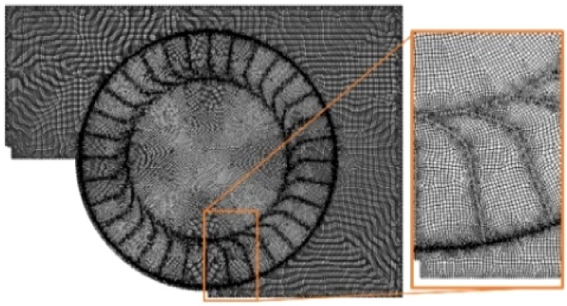

Fig. 2. Visualisation of 123,000 elements mesh.

Table 2. The mesh and timestep independency tests results.

Mesh independency tests results				Timestep independency tests results			
NGS	Elements	Torque (N m)	GCI (%)	NTS	T. size	Torque (N m)	TCI (%)
0	*Infinity*	404.473231	0	0	0 s	202.1165024	0
1	493 000	405.175213	0.014%	1	0.002 s	197.1879831	1.776%
2	123 000	413.859301	0.173%	2	0.004 s	190.2508035	2.591%
4	30 000	529.972714	2.268%	4	0.008 s	173.5491368	6.837%

Richardson extrapolation used in the mesh independency tests; an equation for ratio modification was necessary because time is a one-dimensional unit. In the timestep independency stage, the waterwheel rotation was kept constant for simplifying the testing process.

3. Results and discussion

3.1. Independency test results

The mesh and timestep independency tests used the waterwheel's output torque as the testing variable. The results are summarised in Table 2. From these results, mesh with 123 000 elements was selected for this study because it had a GCI lower than 1%. Moreover, the timestep size of 0.002 s was adopted, which had a timestep convergency index (TCI) of 1.78%. The used mesh distribution is displayed in Fig. 2.

3.2. Waterwheel's simulation results — transient-steady plot

The main difference between the 6-DoF feature with prior dynamic approaches is how the waterwheel or turbine rotates. In 6-DoF, the waterwheel will rotate and accelerate when interacting with water. The rotational acceleration results in a transient period until the waterwheel naturally becomes steady. (The rotational speed is stable). A stable rotational speed will be simultaneous with the torque produced by the wheel. This is because the torque produced by the wheel is balanced (comparable) with the accumulation of preload and moment of inertia of the wheel. Because of this, previous researchers assumed that the simulation results using the 6-DoF feature are closer to the real conditions compared with prior dynamic approaches [16,17]. The simulation results for each preloading case are displayed in Fig. 3.

From the graph in Fig. 3, it is clear there is a dome-shaped part of the transient process from a time ratio of 0 to 0.5. The time ratio is the ratio of the current time to the total time from when the waterwheel starts to rotate until the end of the simulation. The good efficiency of the beginning of the simulation process does not represent the true performance of the waterwheel; although it seems like a true performance graph, the phenomena are only the starting conditions, and waterwheels need more torque to be rotated, which is called a charging effect. This condition was closer to the real condition, which has never been captured in prior dynamic approaches. Furthermore, the charging effect could influence the calculated water distribution in the waterwheel's buckets in the CFD simulation, which

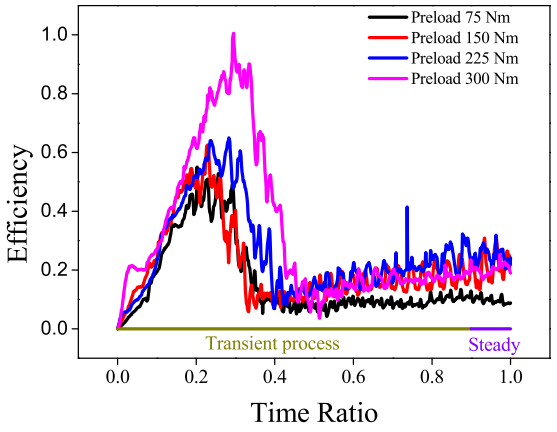

Fig. 3. Efficiency graph of breastshot waterwheel during simulation.

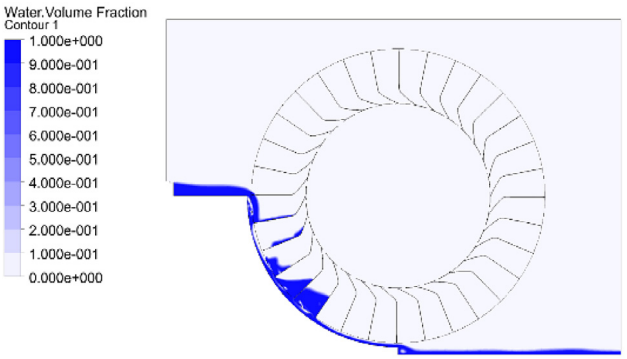

Fig. 4. The water volume fraction contour at top of dome in different cases of 300 N m preload.

could affect the quality of the performance prediction by the CFD method. The true performance characteristic graph can only be obtained by the variance of the preload.

From Fig. 4, it can be observed that, when the waterwheel rotates slowly, water will fill the buckets, generating a great amount of torque on the waterwheel. A high torque results in significant acceleration, causing the turbine speed to be too high. This condition makes the efficiency in the graph drop below 10%. After the charging phenomenon, however, the breastshot waterwheel speed will be normalised and steady.

3.3. Waterwheel's simulation results — steady state performance graph

The obtained values from the simulation results were selected only under the steady condition to obtain the real breastshot waterwheel performance graph for this study. The breastshot waterwheel's performance graph is shown in Fig. 5. Fig. 5 shows that the prediction for the maximum efficiency of the breastshot waterwheel in this study was about 25%, which would be attained at a rotational speed of 6.5 rpm. This waterwheel efficiency is low compared with those of previous studies [8–11] due to too much water flowing outside the waterwheel, as captured in Fig. 4. In contrast, the shape of the graphic and the way the data were obtained are similar to the experimental data in a prior study [11].

4. Conclusion

The CFD simulation of the breastshot waterwheel using the 6-DoF feature could be used for visualising the real phenomenon of the energy conversion process in a breastshot waterwheel turbine. The 6-DoF feature could capture the transient process phenomenon, which also occurred in real conditions but was not calculated by other features

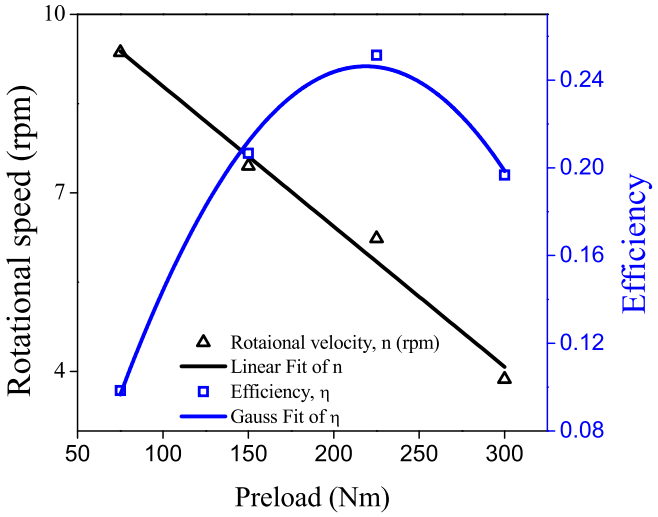

Fig. 5. Real performance after steady.

in the CFD method. The charging effect in the transient process could affect the quality of the numerical simulation. Thus, the 6-DoF feature can be the right choice for breastshot waterwheel turbine simulation.

Acknowledgment

This work supported by the Directorate of Research and Service Community (DRPM) Universitas Indonesia with grant No: 0050/UN2.R3.1/HKP.05.00/2019.

References

[1] Lahimer AA, Alghoul MA, Sopian K, Amin N, Asim N, Fadhel MI. Research and development aspects of pico-hydro power. Renew Sustain Energy Rev 2012;16:5861–78.
[2] Siswantara AI, Budiarso, Prakoso AP, Gunadi GGR, Warjito, Adanta D. Assessment of turbulence model for cross-flow pico hydro turbine numerical simulation. CFD Lett 2018;10:38–48.
[3] Senior J, Wiemann P, Muller G. The rotary hydraulic pressure machine for very low head hydropower sites. In: Hidroenergia conference. 2008, p. 1–8.
[4] Müller G, Kauppert K. Performance characteristics of water wheels. J Hydraul Res 2004;42:451–60.
[5] Williamson SJ, Stark BH, Booker JD. Low head pico hydro turbine selection using a multi-criteria analysis. Renew Energy 2014;61:43–50. http://dx.doi.org/10.1016/j.renene.2012.06.020.
[6] Gotoh M, Kowata H, Okuyama T, Katayama S. Damming-up effect of a current water wheel set in a rectangular channel. In: World renewable energy congress VI. 2000, p. 1615–8. http://dx.doi.org/10.1016/B978-008043865-8/50333-0.
[7] Muller G, Wolter C. The breastshot waterwheel: design and model tests. ICE Proc-Eng Sustain 2004;203–11.
[8] Quaranta E, Revelli R. Performance characteristics, power losses and mechanical power estimation for a breastshot water wheel. Energy 2015;87:315–25. http://dx.doi.org/10.1016/j.energy.2015.04.079.
[9] Quaranta Emanuele, Revelli R. Hydraulic behavior and performance of breastshot water wheels for different numbers of blades. J Hydraul Eng 2016;143. 4016072.
[10] Quaranta E, Revelli R. Optimization of breastshot water wheels performance using different inflow configurations. Renew Energy 2016;97:243–51. http://dx.doi.org/10.1016/j.renene.2016.05.078.
[11] Quaranta E, Revelli R. CFD Simulations to optimize the blade design of water wheels. Drinking Water Eng Sci 2017;10(27).
[12] Warjito, Adanta D, Budiarso, Prakoso AP. The effect of bucketnumber on breastshot waterwheel performance. In: IOP conference series: Earth and environmental science. IOP Publishing; 2018, p. 12031.
[13] Budiarso, Warjito JS, Prakoso AP, Adanta D. Influence of bucket shape and kinetic energy on breastshot waterwheel performance. In: 2018 4th international conference on science and technology (ICST). IEEE; 2018, p. 1–6.
[14] Adanta D, Budiarso Warjito, Siswantara AI. Assessment of turbulence modelling for numerical simulations into pico hydro turbine. J Adv Res Fluid Mech Therm Sci 2018;45:21–31.
[15] Fluent A. Ansys fluent theory guide. USA 15317: ANSYS Inc.; 2011, p. 724–46.
[16] Adanta D, Hindami R, Budiarso Warjito, Siswantara AI. Blade depth investigation on cross-flow turbine by numerical method. In: 2018 4th international conference on science and technology (ICST). Yogyakarta: IEEE; 2018, p. 1–6.
[17] Warjito, Arifianto SA, Budiarso, Nasution SB, Adanta D. Effect of blades number on undershot waterwheel performance with variable inlet velocity. In: 2018 4th international conference on science and technology (ICST). IEEE; 2018, p. 1–6.